ISSN 1063-7745, Crystallography Reports, 2018, Vol. 63, No. 1, pp. 79–83. © Pleiades Publishing, Inc., 2018.
Original Russian Text © A.P. Zhukhlistov, V.M. Novikov, 2018, published in Kristallografiya, 2018, Vol. 63, No. 1, pp. 88–92.

REAL STRUCTURE OF CRYSTALS

Nanohematite from Ferruginous Quartzites of Kursk Magnetic Anomaly According to Transmission Electron Microscopy Data

A. P. Zhukhlistov* and V. M. Novikov

Institute of Geology of Ore Deposits, Petrography, Mineralogy, and Geochemistry, Russian Academy of Sciences, Moscow, 109017 Russia

**e-mail: anzhu@igem.ru*

Received October 20, 2016

Abstract—Transmission electron microscopy study of ferruginous quartzite (jaspilites) from the Lebedinsky field of Kursk magnetic anomaly has revealed for the first time hematite nanoformations (about 10 nm in size), sp. gr. $R\bar{3}$, which coexist with hematite, sp. gr. $R\bar{3}c$, in the same crystallographic orientation or manifest themselves as individual nanoinclusions in the substrate of poorly crystallized magnetite. On the assumption that, in correspondence with the energy-dispersive X-ray analysis data, octahedral sites in the hematite structure can be occupied by only Fe cations, several structural models are proposed explain the hematite symmetry lowering to $R\bar{3}$.

DOI: 10.1134/S1063774518010224

INTRODUCTION

The crystal structure of hematite α-Fe_2O_3 is a hexagonal close-packed arrangement of oxygen atoms along the [0001] direction, 2/3 octahedral voids of this structure are filled with Fe^{3+} cations according to the corundum motif (cation site *A* with coordinates 0, 0, 0.355) [1, 2]. The hematite structure is described within the space group $R\bar{3}c$; the hexagonal lattice parameters are $a = 5.038$ Å and $c = 13.772$ Å [2].

The Rietveld method was used in [3] to analyze the reflection profile in the diffraction patterns of powder hematite samples recorded using synchrotron radiation. Proceeding from the broadening of some groups of *hkl* reflections, the trigonal symmetry of hematite was found to be lowered to monoclinic $C2/c$. The relative distortions of monoclinic lattice parameters in comparison with the parameters obtained by hexagonal lattice transformation are on the order of 10^{-4}. A decrease in the parameter *b* and an increase in the parameter *a* of the monoclinic cell were observed.

Oxygen atoms in hematite can partially be replaced with OH^- ions; this replacement is accompanied by the generation of vacancies in octahedra for preserving the charge balance. These Fe-deficient hematites, described by the general formula $Fe_{2-x/3}(OH)_xO_{3-x}$, are referred to as hydrohematites ($1 \le x < 0.5$) or protohematites ($0.5 \le x < 0$) [4]. The most complete structural data on OH-containing hematite were obtained from the X-ray diffraction study of the intermediate phases, formed as a result of thermal and hydrothermal transformations of iron hydroxides, such as goethite (α-FeOOH) and akaganeite (β-FeOOH). Modeling of the diffraction features and refinement of structures were performed mostly within the sp. gr. $R\bar{3}c$ [4, 5]. In [6], based on the IR and Raman spectroscopy data, symmetry lowering to $R3c$ was revealed for protohematite; this lowering is related to the structural distortions caused by the replacements of oxygen atoms with OH^- hydroxyl groups. The monoclinic sp. gr. $I2/a$ was revealed in [7] as a result of Rietveld refinement of the hydrohematite structure based on powder diffraction data recorded in situ using synchrotron radiation when studying the transformation of akaganeite into hematite. The break of trigonal symmetry was evidenced by the splitting of some diffraction peaks. Thus, the decrease in the trigonal symmetry to monoclinic, established for hematite [3] and hydrohematite [7], manifests itself as broadening or small splitting of reflections in powder X-ray diffraction patterns.

In this study, we revealed for the first time (using transmission electron microscopy (TEM)) the presence of nanoinclusions of hematite with the $R\bar{3}$ symmetry in hematite samples from ferruginous quartzite of Kursk magnetic anomaly (KMA) based on selected area diffraction patterns and high-resolution TEM images. Structural models of hematite are proposed to explain the lowering of its symmetry.

EXPERIMENTAL

We performed a TEM study of the hematite from oxidized ferruginous quartzites (jaspilites) of the Leb-

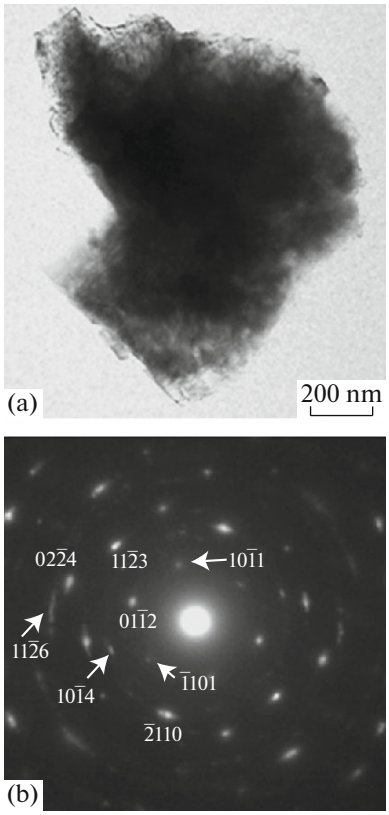

Fig. 1. (a) TEM image of hematite particle and (b) the corresponding electron diffraction pattern.

edinsky field of KMA; these minerals form the most important component of the Precambrian orogenesis [8]. The ore-forming minerals of the initial and oxidized jaspilites are magnetite, hematite, and siderite [9].

Hematite samples were analyzed in a JEM-2100 transmission electron microscope (JEOL, Japan) at an accelerating voltage of 200 kV, using an X-Max detector for energy-dispersive X-ray microanalysis (Oxford Instruments, United Kingdom). Lattice images and electron diffraction patterns were recorded by a CCD camera using the Digital Micrograph package (Gatan, United States). Fourier spectra were obtained for high-resolution images applying the Digital Micrograph and Crisp programs (Sweden). Electron diffraction patterns were simulated with the aid of the eMap program (Sweden). A low-intensity electron beam was applied to reduce to minimum possible sample amorphization under electron beam irradiation.

Samples were prepared from aqueous suspensions obtained by short-term ultrasonic treatment of minerals, with subsequent evaporation of suspension drops onto the supporting film. High-resolution images were obtained from thin edges of particles.

RESULTS AND DISCUSSION

According to the TEM data, hematite is mainly presented by monomineral segregations. The diffraction patterns from the chosen region are characterized by point reflections, corresponding basically to one orientation (or, more rarely, two different orientations) of particles with respect to the electron beam axis. An analysis of high-resolution images revealed the presence of magnetite nanoinclusions for some hematite particles. Hematite can form (as a secondary mineral) siderite pseudomorphs. Obviously, the presence of these mineral associations is a manifestation of the complex processes of transformation of mineral phases. According to the energy-dispersive data, hematite particles have a similar elemental composition, with dominance of Fe and small amounts of Si and (sometimes) Al impurities.

A very interesting finding is the hematite nanoformations, whose diffraction features indicate lowering of hematite symmetry. Figure 1a presents a TEM image of a hematite particle. The electron diffraction pattern from the chosen region of this particle (Fig. 1b), belonging to the $[0\bar{1}11]$ axis zone, contains, along with the reflections corresponding to the interplanar spacings d_{hkl} = 3.69 (reflection $01\bar{1}2$), 2.52 ($\bar{2}110$, $11\bar{2}0$), 2.21 ($11\bar{2}3$), and 1.84 Å ($02\bar{2}4$), weak reflections corresponding to d_{hkl} = 4.16 Å. These reflections also belong (with regard to the d_{hkl} value and their position) to this zone and have indices $10\bar{1}1$ and $\bar{1}101$, which are forbidden in the sp. gr. $R\bar{3}c$ but allowed in the sp. gr. $R\bar{3}$. The electron diffraction patterns contain, along with the reflections belonging to the aforementioned zone, some other hematite reflections: $11\bar{2}0$, which corresponds to crystallites with another orientation; $10\bar{1}4$ (d_{hkl} = 2.70 Å); and $11\bar{2}6$ (d_{hkl} = 1.69 Å. This pattern is an evidence of orientational inhomogeneity of the subparticles forming this particle. According to the energy-dispersive data, the empirical formula of hematite can be written as $Fe_{1.98}Si_{0.02}O_3$.

More details on the specific features of the hematite phase $R\bar{3}$ were obtained by analyzing high-resolution images. The images in Figs. 2a and 2b contain lattice fringes with interplanar spacings of 2.52 and 3.69 Å, related to the hematite planes ($\bar{2}110$) and ($01\bar{1}2$), respectively. These fringes may be observed separately or intersect at right angle, indicating their affiliation to the $[0\bar{1}11]$ axis zone of hematite. A characteristic feature of these images is the presence of a nanoformation 15 nm in size, with lattice fringes related to the ($\bar{2}110$) and ($01\bar{1}2$) planes, making a right angle. There are fringes with d = 4.16 Å in the central part of the images; they also correspond to the $[0\bar{1}11]$ axis zone of hematite and are related to the

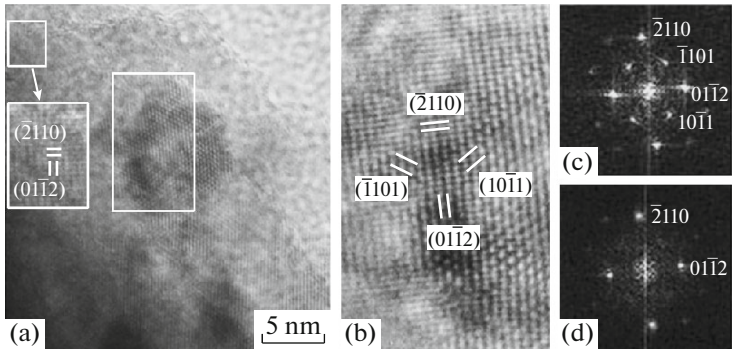

Fig. 2. Hematite particle: (a) high-resolution TEM image (the area selected by a thin white line in the upper left corner is shown on the enlarged scale in the inset); (b) enlarged image of hematite nanoformation, selected by a bold white line in panel a; and (c, d) two-dimensional Fourier spectra of the (c) central and (d) peripheral regions of the nanoformation.

$(10\bar{1}1)$ and $(\bar{1}101)$ planes. Figures 2c and 2d show, respectively, the Fourier spectra for the central and peripheral regions of the hematite nanoformation, which correspond to the diffraction patterns from the $[0\bar{1}11]$ axis zone of hematite phases $R\bar{3}$ and $R\bar{3}c$.

The hematite lattice fringes in the high-resolution image in Fig. 3a manifest themselves nonuniformly. In particular, the upper part of the image is characterized by one-dimensional lattice fringes, corresponding to the $(11\bar{2}0)$ hematite planes with different azimuthal orientations and the $(01\bar{1}2)$ plane. Their manifestation domain has a size of 5–10 nm. The lower part of the image contains nanoregions with equally oriented two-dimensional fringes with interplanar spacings of 2.70 and 2.20 Å, which correspond to the $(0\bar{1}14)$ and $(\bar{1}\,\bar{1}23)$ planes of hematite and are related (according to their mutual position) to the $[\bar{2}3\bar{1}1]$ zone. Among two-dimensional lattice fringes, there is a nanoformation about 10 nm in size (shown by a dotted line in Fig. 3a), which contains, along the aforementioned lattice fringes, fringes with d = 4.16 Å. According to their location, they are related to the $(10\bar{1}1)$ plane of the $[\bar{2}3\bar{1}1]$ axis zone (Fig. 3b) and indicate the $R\bar{3}$ symmetry of the hematite nanoformation. Figures 3c and 3d show the Fourier spectra for this nanoformation and the adjacent region, which correspond to the diffraction patterns from the $[\bar{2}3\bar{1}1]$ axis zone of hematite phases $R\bar{3}$ and $R\bar{3}c$.

The high-resolution images show that the hematite phase $R\bar{3}$ in the particle manifests itself only in the form of local nanoformations, surrounded by the hematite phase with the symmetry $R\bar{3}c$; these phases have the same crystallographic orientation. Thus, the electron diffraction pattern presented in Fig. 1b can be interpreted as a mixture of two hematite phases with symmetries $R\bar{3}c$ and $R\bar{3}$, with dominance of the former phase.

Local manifestation of nanohematite phase $R\bar{3}$ was also observed in the high-resolution images of a particle composed of magnetite Fe_3O_4 and siderite $FeCO_3$ (Fig. 4a). In the electron diffraction pattern (Fig. 4b), the reflections in the form of short arcs, $\bar{1}11$ (d = 4.84 Å), 220 (d = 2.97 Å), 113 (d = 2.52 Å), and 440 (d = 1.48 Å), which are due to the $[\bar{1}\bar{2}1]$ axis zone, correspond to magnetite, and point reflections $11\bar{2}0$ (d = 2.34 Å) and $2\bar{1}\bar{1}6$ (d = 1.73 Å), which are due to the $[\bar{2}201]$ axis zone, correspond to siderite. The high-resolution image from the particle edge (Figs. 4c, 4d) demonstrates a nanoformation about 10 nm in size, with lattice fringes whose position and d_{hkl} values

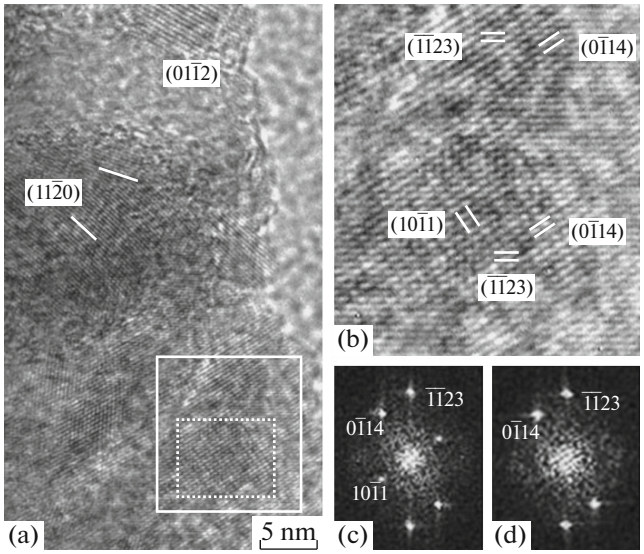

Fig. 3. Hematite particle: (a) high-resolution TEM image (white dashes show the orientation of $(01\bar{1}2)$ planes of hematite), (b) enlarged image of the area selected by a solid white line in panel a, and (c, d) two-dimensional Fourier spectra from (c) the area selected by a dotted line in panel a and (d) the adjacent area located above it.

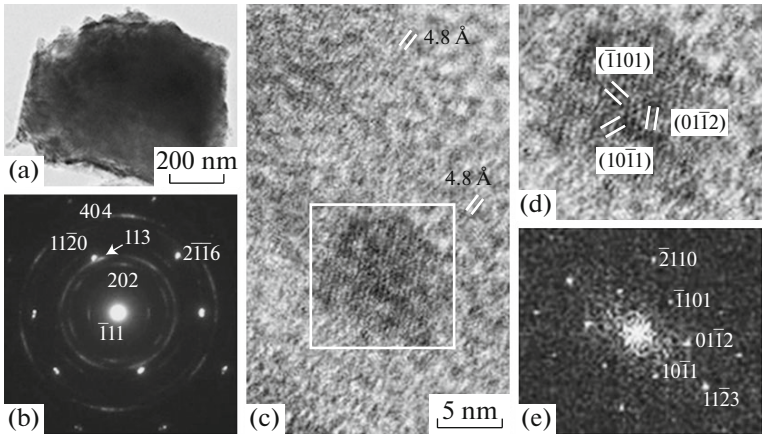

Fig. 4. TEM data on a particle formed by association of magnetite and siderite: (a) particle image, (b) corresponding electron diffraction pattern, (c) high-resolution TEM image of the particle edge, (d) enlarged image of the hematite nanoparticle selected in panel c, and (e) two-dimensional Fourier spectrum from the selected area.

(4.15 and 3.70 Å) correspond to the $(10\bar{1}1)$, $(\bar{1}101)$, and $(01\bar{1}2)$ planes of the $[0\bar{1}11]$ axis zone of hematite phase $R\bar{3}$. The Fourier spectrum of the hematite nanoformation (Fig. 4e) corresponds to the diffraction pattern from the $[0\bar{1}11]$ axis zone of hematite phase $R\bar{3}$. Short bent fringes with an interplanar spacing of ~4.8 Å are observed in the image of the particle edge (Fig. 4c) near nanohematite; obviously, these fringes are related to the poorly crystallized magnetite phase. The particle consists mainly of Fe, with small amounts of Si and Ca impurities.

The aforementioned specificity of the manifestation of hematite phase $R\bar{3}$ indicates that it can be formed in two ways. In one case, nanoformations of hematite phase $R\bar{3}$ are associated with hematite $R\bar{3}c$. These phases have the same crystallographic orientation, which may indicate the formation of nanohematite $R\bar{3}$ over hematite $R\bar{3}c$. In the other case, hematite phase $R\bar{3}$ is a nanoinclusion in the substrate of poorly crystallized magnetite. This fact is an evidence of different processes of transformation of initial minerals, which accompany the formation of hematite phase $R\bar{3}$. Obviously, the aforementioned existence of hematite phase $R\bar{3}$ only in the form of individual nanoformations suggests its low stability.

The occurrence of the $h\bar{h}0l$ reflections with $l = 2n + 1$ (which are forbidden in the sp. gr. $R\bar{3}c$) in the diffraction patterns of nanohematite can be explained within two structural models of hematite phase $R\bar{3}$, on the assumption (in correspondence with the energy-dispersive data) that the octahedral sites can be occupied by only Fe cations. In the first model, two octahedral sites, *A* (0, 0, 0.355) and *B* (0, 0, 0.145), can be nonequivalent if one of them is preferably occupied by cation vacancies, formed during partial hydration of hematite and replacement of oxygen atoms with hydroxyl groups OH^-.

The second model suggests partial replacement of Fe^{3+} cations with Fe^{2+} cations, with some increase in the Fe^{2+} content for preserving the charge balance. Fe^{2+} cations can fill larger octahedral voids according to the anticorundum motif (nonequivalent cation sites *C* (0, 0, 0) and *D* (0, 0, 0.5) in the sp. gr. $R\bar{3}$). In this case, the nonequivalence of octahedral sites may be due to both the deficit of Fe^{3+} cations in site *A* or *B* and the preferred occupation of one of the *C* or *D* sites with Fe^{2+} cations. A comparison of the structural factors for the $01\bar{1}2$ and $10\bar{1}1$ reflections, calculated within these models, with their intensities in the electron diffraction patterns showed some preference for the second model. In particular, the ratio of the structural factors for the $01\bar{1}2$ and $10\bar{1}1$ reflections within the first model is 6.8, with the occupancy one of octahedral sites (*A* or *B*) with Fe^{3+} cations equal to 0.8 (composition $Fe_{1.8}(OH)_{0.6}O_{2.4}$). For the second model, with the cation composition $Fe^{3+}_{1.8}Fe^{2+}_{0.3}$, this ratio ranges from 1.4 to 3.5, depending on the character of occupation of nonequivalent octahedral sites *A*, *B* and *C*, *D* with Fe^{3+} and Fe^{2+} cations, respectively. The second model takes into account possible reduction of Fe^{3+} in hematite, in particular, under influence of dissimilatory iron-reducing microorganisms, which are believed to be involved in the formation of ferruginous quartzite [10] and the formation of hematite over magnetite in later oxidative processes [11, 12].

CONCLUSIONS

The existence of nanohematite with the $R\bar{3}$ symmetry in the mineral composition of ferruginous quartzites of the Lebedinsky field of KMA was

revealed for the first time by TEM analysis. High-resolution TEM images showed that the hematite phase $R\bar{3}$ forms local nanoformations (~10 nm in size), which coexists with hematite phase $R\bar{3}c$ (having the same crystallographic orientation) or manifests itself as individual nanoinclusions in the substrate of poorly crystallized magnetite. Two structural models of hematite phase $R\bar{3}$ were proposed on the assumption that octahedral sites in the hematite structure can be occupied by only Fe cations. In the first model, cation vacancies formed as a result of partial hydration of hematite and replacement of oxygen atoms with hydroxyl groups OH^- are regularly located in one of two nonequivalent octahedral sites. According to the second model, Fe^{3+} cations are partially replaced with Fe^{2+} cations, with preferred occupation of Fe^{3+} and/or Fe^{2+} nonequivalent octahedral sites according to corundum and anticorundum (carbonate) motifs, respectively.

ACKNOWLEDGMENTS

The study was performed within State contract no. 0136-2014-0009.

REFERENCES

1. N. V. Belov, *Structure of Ionic Crystals and Metal Phases* (Izd-vo AN SSSR, Moscow, 1947) [in Russian].
2. R. L. Blake, R. E. Hessevick, T. Zoltai, et al., Am. Mineral. **51**, 123 (1966).
3. R. Przenioslo, I. Sosnowska, M. Stękiel, et al., Physica B **449**, 72 (2014).
4. E. Wolska and U. Schwertmann, Z. Kristallogr. **189**, 223 (1989).
5. A. Gualtieri and P. Venturelli, Am. Mineral. **84**, 895 (1999).
6. E. B. Burgina, G. N. Kustova, S. V. Tsybulya, et al., Zh. Strukt. Khim. **41** (3), 489 (2000).
7. K. M. Peterson, P. J. Heaney, J. E. Post, et al., Am. Mineral. **100**, 570 (2015).
8. N. I. Golivkin, N. L. Kononov, V. P. Orlov, et al., *Iron Ores of Kursk Magnetic Anomaly* (Geoinformmark, Moscow, 2001) [in Russian].
9. A. P. Zhukhlistov and V. M. Novikov, Crystallogr. Rep. **61** (6), 987 (2016).
10. D. G. Zavarzina, Paleontol. J., No. 6, 585 (2004).
11. L. E. Lagoeiro, J. Metamorph. Geol. **16**, 415 (1998).
12. P. F. Barbosa and L. Lagoeiro, Am. Mineral. **95**, 118 (2010).

Translated by Yu. Sin'kov